Palladium-tin catalysts for the direct synthesis of H_2O_2 with high selectivity

Simon J. Freakley*[,a,†], Qian He,[b,c,†] Jonathan Harrhy,[a] Li Lu,[b] David A. Crole,[a] David J. Morgan,[a] Edwin N. Ntainjua,[a] Jennifer. K. Edwards,[a] Albert F. Carley,[a] Albina Borisevich,[c,d] Christopher J. Kiely [b] and Graham J. Hutchings*[a]

[a] Cardiff Catalysis Institute and School of Chemistry, Main Building, Park Place, Cardiff, CF10 3AT, UK

[b] Department of Materials Science and Engineering, Lehigh University, 5 East Packer Avenue, Bethlehem, PA 18015-3195, USA

[c] Materials Science and Technology Division, Oak Ridge National Laboratory, Oak Ridge, Tennessee 37831, USA

[d] Center for Nanophase Materials Sciences, Oak Ridge National Laboratory, Oak Ridge, Tennessee 37831, USA

[†] These authors have equal contribution

* Corresponding Authors:- hutch@cf.ac.uk , freakleys@cf.ac.uk

Abstract

The direct synthesis of hydrogen peroxide (H_2O_2) from H_2 and O_2 represents a potentially atom efficient alternative to the current industrial indirect process. We show that the addition of tin to palladium catalysts coupled with an appropriate heat treatment cycle switches-off the sequential hydrogenation and decomposition reactions, enabling selectivities of >95% towards H_2O_2. This effect arises from a tin oxide surface layer that encapsulates small Pd-rich particles while leaving larger Pd-Sn alloy particles exposed. We show this effect is a general feature for oxide supported Pd catalysts containing an appropriate second metal oxide component and we set out the design principles for producing high selectivity Pd-based catalysts for direct H_2O_2 production that do not contain Au.

Currently, the demand for H_2O_2 is met by an indirect process, which produces H_2O_2 through the sequential hydrogenation and oxidation of a substituted anthraquinone (*1*). For economic reasons, the process is operated at large scale and produces concentrated H_2O_2. In reality, many applications, such as disinfection and water purification, require only dilute H_2O_2 which means that concentrated H_2O_2 has to be diluted at the point of use. Research into the direct synthesis of H_2O_2 from H_2 and O_2 as a more suitable solution to small-scale, on-site H_2O_2 production has focused on palladium (Pd)-based catalysts (*2-4*). However, H_2O_2 is itself highly reactive and the presence of H_2 favors hydrogenation and decomposition reactions that form water. The addition of strong acids and halides into the reaction medium can suppress the sequential hydrogenation and degradation in supported Pd catalysts (*5*); but can also promote metal leaching and requires further purification of the H_2O_2 before use.

Bimetallic Au-Pd alloy catalysts have been extensively studied as catalysts for the direct H_2O_2 synthesis reaction on a number of support materials including TiO_2, SiO_2 and activated carbon (*6-9*). Comparable yields to monometallic Pd catalysts can be achieved without the need for acid and halide additives in the reaction mixture, and 95% selectivity to H_2O_2 could be achieved with Au-Pd alloy nanoparticles (NPs) dispersed on an acid pre-treated activated carbon support material (*10*). Hydrogen peroxide hydrogenation could be decoupled from H_2O_2 synthesis with an acid pre-treatment that blocked sites on the carbon support material responsible for H_2O_2 degradation. Although this approach was very successful on an activated carbon support material, the same blocking effect could not be fully achieved on other commercial support materials such as SiO_2 and TiO_2.

As O_2 dissociation is undesirable in the direct synthesis of H_2O_2, the reaction can be treated as a selective hydrogenation of O_2. We explored other Pd-metal combinations that are used for selective hydrogenation reactions as potential catalysts for H_2O_2 synthesis, focusing on non-precious metal to lower costs. Tin has been used to modify hydrogenation catalysts in reactions such as the selective hydrogenation of 1-3 butadiene (*11*). Further examples have been reported for the liquid phase hydrogenation of hexa-1-3-diene and hexa-1-5-diene (*12*), as well as the hydrogenation of unsaturated alcohols (*13*). The addition of Sn to Pd or Pt can alter the behavior of the catalyst during hydrogenation reactions and, in particular, may have an effect on subsequent reactions of the products with the catalyst.

We report the development of tin-containing palladium catalysts on commercially available TiO_2 and SiO_2 supports that can achieve > 95% selectivity toward direct H_2O_2 synthesis. These catalysts, after being subjected to an appropriate heat treatment regimen, obviate the need for pre-treating the support with acids, and contain far less precious metal than Au-Pd catalysts. Furthermore, we present the general principles whereby high selectivity catalysts can be obtained with other Pd-metal combinations.

Simple impregnation of gold and palladium metal salts onto many catalyst supports has been shown to generate highly active catalysts for direct H_2O_2 synthesis. In addition, high-temperature calcination or reduction treatments are known to be crucial to improve the stability of the catalyst. As a starting point, we used this simple catalyst preparation methodology to prepare a 2.5wt% Pd- 2.5wt% Sn / TiO_2 catalyst as well as its monometallic analogs (*8, 10*). A synergistic effect toward the direct synthesis of H_2O_2 was observed when both metals were present compared to the analogous monometallic catalysts after calcination in static air at 500 °C for 3 h (Table S1) (*14*). The activity of this 2.5wt% Pd - 2.5wt% Sn / TiO_2 catalyst (62 mol kg^{-1} h^{-1}) is similar to that of a 2.5wt% Pd - 2.5wt% Au / TiO_2 catalyst (*8*) (*i.e.* 64 mol kg^{-1} h^{-1}) . We then optimized the ratio of Sn-to-Pd while maintaining a total metal content of 5wt% (Table S2) (14), and found an optimum nominal composition, 3wt% Pd - 2 wt% Sn / TiO_2, that exhibited an H_2O_2 productivity of 68 mol kg^{-1} h^{-1} (Table 1, entry 1). By comparison, the H_2O_2 degradation activity of the optimized Sn-Pd catalyst was very low compared to that reported for Au-Pd systems (65 mol kg^{-1} h^{-1} for 3wt% Pd - 2 wt% Sn / TiO_2 versus 235 mol kg^{-1} h^{-1} for 2.5wt% Pd - 2.5wt% Au / TiO_2) which indicated that Sn is also playing a beneficial role in preventing the over hydrogenation/decomposition of H_2O_2. However, the Sn-Pd catalysts calcined at 500 °C for 3 h under static air were unstable to multiple reaction cycles (Table 1, entry 1).

The nature of the catalyst surface and in particular the oxidation states of the active metal are crucial to obtaining high selectivity. Therefore characterization of this 3wt% Pd - 2 wt% Sn / TiO_2 catalyst after calcination by X-ray photoelectron spectroscopy (XPS) was carried out and showed the majority of the surface Pd was present as Pd^{2+} while the Sn Auger parameter showed that SnO_2 was present in the calcined catalyst (Figure S1, Table S3) (14). Analysis of the nanostructure of this catalyst using scanning transmission electron microscopy – high angle annular dark filed imaging (STEM-HAADF) and electron

energy loss spectroscopy (EELS) revealed that the SnO_x was present as a thin (< 2 nm thick) amorphous film coating the TiO_2 support particles (Fig. 1, A to D, and Fig. S2 (*14*)). A population of 5 - 10 nm NPs were also present in the sample that contained a homogeneous mixture of both Pd and Sn (Figures 1(a)-(d) and S3 (*14*)). Lattice fringe fitting of these particles strongly suggests a metallic Pd-Sn alloy structure rather than segregated or mixed oxides meaning that only the surface of the particles is oxidised. Many sub-2 nm Pd-rich NPs were also observed and were often associated with the SnO_x thin films, and because these species were much less numerous in a 5wt% Sn-only / TiO_2 sample (Figure S4) (*14*), they were primarily associated with the PdO_x component in the bimetallic catalyst.

A limiting factor in achieving high selectivity towards H_2O_2 with Au-Pd / TiO_2 catalysts prepared by the wet impregnation method is that the catalysts exhibit a variation in composition with particle size, with the smallest particles being Pd-rich (*9*). These small Pd-rich NPs are likely to be highly active for H_2O_2 synthesis and also for its subsequent hydrogenation/decomposition, as has been shown when Au-Pd catalysts are prepared by colloidal techniques with particle sizes typically 2 to 4 nm(*15*). In the case of the Sn-Pd system, the small Pd-rich NPs are often associated with the amorphous SnO_x films. We postulated that it might be possible to further decrease the H_2O_2 degradation activity of the catalyst by inducing encapsulation of the ultra-small Pd-rich NPs by this SnO_x film. We therefore used subsequent thermal treatments in an attempt to induce a strong-metal-support-interaction (SMSI) between the Pd and SnO_x layer (*16-21*). We first added a low-temperature reduction step (200 °C, 2 h, 5% H_2 in Ar), which made the catalysts stable to multiple reaction cycles (Table 1, entry 2). However, the H_2O_2 degradation activity increased markedly from 65 to 300 mol kg^{-1} h^{-1}, which was associated with the reduction of Pd^{2+} to metallic Pd, as shown by XPS, (Table S3, Figure S1) (*14*). Metallic Pd is known to be a more effective H_2O_2 hydrogenation catalyst (*7*).

Detailed STEM analysis of this reduced sample was carried out to investigate any structural changes in the sample on reduction (Figures S5 and S6) (*14*). Analysis identified the presence of thin SnO_x films, sub-2 nm Pd NPs, and 5 to 10 nm NPs whose lattice fringe spacings and angles were consistent with Pd-Sn metallic alloy phases. We then re-oxidized, this reduced catalyst to restore Pd^{2+} as the predominant surface species (as confirmed by XPS (Figure S1, Table S3)) (*14*) and complete an oxidation-reduction-

oxidation (O-R-O) cycle with the aim of encapsulating the small Pd species and re-generating the oxidised Pd-Sn surface on the larger NPs. Re-oxidizing the reduced catalyst for various time periods at 400 °C under static air had little effect on the H_2O_2 synthesis productivity, but markedly decreased the H_2O_2 degradation activity (Fig. 2A). After a 4 h re-oxidation treatment, the catalyst showed no activity toward H_2O_2 degradation and could produce H_2O_2 with an H_2 selectivity of > 95% (Table 1, entry 3). This catalyst was stable to multiple reaction cycles and showed negligible leaching of Sn (0 ppb) or Pd (2 ppb) during a 30 min reaction as measured by ICP-MS. This re-oxidized 3wt% Pd - 2wt% Sn / TiO_2 catalyst was subjected to further H_2O_2 testing including multiple sequential H_2O_2 synthesis tests (Fig. 2B). After running the reaction consecutively 5 times, the H_2O_2 concentration increased linearly to 0.53wt%, retaining both the high H_2O_2 synthesis and zero H_2O_2 degradation rates. This result implies that no subsequent decomposition or hydrogenation reactions of H_2O_2 took place with this catalyst. The re-oxidized 3wt% Pd - 2wt% Sn / TiO_2 catalyst was also tested for H_2O_2 degradation with varying concentrations of H_2O_2 under a pressure of 5% H_2 / CO_2 (Fig. 2C) and showed no degradation of H_2O_2 in solutions of up to 8 wt%, whereas the corresponding Au-Pd / TiO_2 catalyst showed substantially higher H_2O_2 degradation activity at all of the concentrations studied.

The nanostructure of the catalyst after the oxidation-reduction-oxidation treatment was characterized to identify any structural changes that could be responsible for the observed high selectivity. Three structures were again revealed to be present in the catalyst–amorphous SnO_x films on the TiO_2 particles, small Pd species associated with these films, and larger Pd-Sn NPs (Fig. 1, E to H, and Figures S7 and S8 (*14*)).

Detailed EELS analysis of the thin film regions (Figure S9 (*14*)) after various heat treatments indicates the presence of SnO_x films which can be either reduced or oxidised depending on the final heat treatment stage as indicated by the absence/presence of the O K edge in the EELS spectrum. In contrast to the thin films, EELS analysis of Sn-Pd nanoparticles (Figure S10 (*14*)) at different stages of the heat treatment cycle show no clear O K edge. This confirms these nanoparticles to be metallic Pd-Sn alloys, at least in the bulk, which is also consistent with the lattice fringe fitting. Some slight oxidation of the surface of these particles is possible as detected by our XPS measurements, but at such a level that is below the detectability limit of the EELS measurements. The 3wt% Pd – 2wt% Sn / TiO_2 catalyst after the oxidation-

reduction-oxidation cycle shows evidence that the small Pd-rich particles NPs responsible for high hydrogenation activity often appear to be encapsulated in the amorphous SnO_x layer (Figure S11 (*14*)). We suggest that by generating strong metal-support interactions (SMSI) that can effectively 'bury' the population of smaller Pd-rich NPs, the H_2O_2 degradation activity of the catalyst is limited (Fig. 3A). The larger uncovered Pd-Sn alloy NPs are then mainly responsible for the H_2O_2 production and are inherently less prone to cause subsequent H_2O_2 degradation than Pd-Au NPs. The monometallic Pd / TiO_2 catalyst that was subjected to the optimized oxidation-reduction-oxidation cycle (Table S4, entries (1-2) (*14*)) did not induce this effect, confirming that the amorphous layer responsible for SMSI is not TiO_2 based.

To investigate if this effect was unique to the 2wt% Sn - 3wt%Pd / TiO_2 catalyst, similar heat treatment protocols were applied to the analogous 2.5wt% Au -2.5wt% Pd / TiO_2 system. The catalytic results (Table 1, entries 4-6) show that the same suppression of H_2O_2 degradation was also not observed for a corresponding oxidized-reduced-oxidized Au-Pd / TiO_2 catalyst. Results obtained for monometallic Pd and bimetallic Sn-Pd catalysts (Table S4, entries 3-5) (*14*) also indicate that the reduction step is crucial, as three oxidative treatments fail to induce the effect. It should also be noted that the 200°C reduction temperature used in this study is much lower than that typically reported to induce SMSI effects in TiO_2-only supported catalyst systems (*22*). To demonstrate the proposed SMSI effect with SnO_2, a 'model' 5wt% Pd / SnO_2 catalyst was also prepared and studied by electron microscopy. In the oxidized state, EELS mapping showed the PdO_x particles appear to be clean (Fig. 3B, Figs. S12, S13 (*14*)), whereas after the oxidation-reduction-oxidation treatment the Pd particles show clear evidence of an SnO_x overlayer (Fig. 3C, and Figs. S14, S15 (*14*)).

Further evidence that the suppression of the H_2O_2 degradation does not originate from encapsulation of small Pd particles by TiO_2 but is an SMSI effect arising from the secondary SnO_x component was obtained by using a non-reducible SiO_2 support in place of the TiO_2. When the ratio of Sn : Pd on SiO_2 was optimized (Table S5) (*14*) and the same oxidation-reduction-oxidation heat treatment regimen was applied (Table 1, entries 7-9), the resulting 1wt% Pd – 4wt% Sn / SiO_2 catalyst produced H_2O_2 at a rate of 50 mol kg^{-1} h^{-1} (Table 1, entry 9) and showed no activity toward subsequent H_2O_2 degradation. This 1wt% Pd – 4wt% Sn / SiO_2 catalyst showed no propensity to decompose or hydrogenate H_2O_2 even in

solutions containing up to 12wt% H_2O_2 (Figure S16) (*14*). Furthermore, the catalytic performance of the 1wt% Pd – 4wt% Sn / SiO_2 material was stable through multiple uses (Table S5) (*14*). XPS analysis (Figure S1, Table S4) (*14*) and electron microscopy characterization (Figures S17 and S18) (*14*) of the 1wt% Pd – 4wt% Sn / SiO_2 catalyst showed analogous compositional and structural features (*i.e.* (i) amorphous SnO_x films and associated ultra-small Pd-rich NPs and (ii) larger Pd-Sn alloy particles) as its 3wt% Pd - 2wt% Sn / TiO_2 counterpart.

Our approach of encapsulating small Pd-rich species generated by wet impregnation preparations with secondary oxides canbe generalized if the second metal oxide added to the Pd/primary oxide (*e.g.* TiO_2/SiO_2) support system (i) shows no decomposition activity towards H_2O_2 when in oxide form, (ii) forms an alloy or mixed oxide phase with Pd, and (iii) can encapsulate small Pd-rich particles by SMSI. Based on these design rules and a using a nominal composition of 0.5wt% Pd - 4.5wt% M / TiO_2 that had been subjected to the optimised oxidation-reduction-oxidation treatment, we synthesized a series of bimetallic catalysts where M = Ni, Zn, Ga, In and Co. All of these catalysts showed activity for H_2O_2 synthesis (between 30-64% of that displayed by the Sn-Pd catalyst) and no activity for H_2O_2 degradation (Table S6) (*14*). Thus, our approach opens up the possibility of designing reusable catalysts with greatly reduced precious metal content while still retaining high selectivity to H_2O_2.

References

1. J. K. Edwards, G. J. Hutchings, *Angew. Chem. Int. Ed.* **47**, 9192 (2008).
2. H. Henkel, W. Weber. (US Patent 1,108,752, 1914).
3. J. H. Lunsford, *J. Catal.* **216**, 455 (2003).
4. D. P. Dissanayake, J. H. Lunsford, *J. Catal.* **206**, 173 (2002).
5. V. R. Choudhary, C. Samanta, P. Jana, *Appl. Catal. A-General* **317**, 234 (2007).
6. J. K. Edwards *et al.*, *Catal. Sci. Technol* **3**, 812 (2013).
7. J. K. Edwards *et al.*, *J. Catal.* **292**, 227 (2012).
8. J. K. Edwards *et al., J. Catal.* **236**, 69 (2005).
9. J. K. Edwards, S. J. Freakley, A. F. Carley, C. J. Kiely, G. J. Hutchings, *Acc. Chem. Res.* **47**, 845 (2014).
10. J. K. Edwards *et al.*, *Science* **323**, 1037 (2009).
11. K. Pattamakomsan *et al.*, *Catal. Today* **164**, 28 (2011).
12. E. A. Sales, J. Jove, M. de Jesus Mendes, F. Bozon-Verduraz, *J. Catal.* **195**, 88 (2000).
13. J. P. Stassi, P. D. Zgolicz, S. R. de Miguel, O. A. Scelza, *J. Catal.* **306**, 11 (2013).
14. Supporting information is avaliable online (Experimental details, Tables S1-6, Figures S1 – 18, and references 23-25)
15. J. Pritchard *et al.*, *Langmuir* **26**, 16568 (2010).
16. S. J. Tauster, S. C. Fung and R. L. Garten, *J. Am. Chem. Soc.* **100**, 170 (1978).
17. G. L. Haller and D. E. Resasco, *Adv. Catal*. **36**, 173 (1989).
18. Q. Fu and T. Wagner, *Surf. Sci. Rep.* **62**, 431 (2007).
19. D. W. Goodman, *Catal. Lett*. **99**, 1 (2005).
20. S. J. Tauster, *Acc. Chem. Res.* **20**, 389 (1987).
21. J. Liu, *Chem. Cat. Chem*. **3**, 934 (2011).
22. Q. Fu, T. Wagner, S. Olliges and H-D. Carstangen, *J. Phys. Chem. B* **109**, 944, (2005).
23. L. Kover *et al.*, *J. Vac. Sci. Technol. A-Vac. Surf. Films* **13**, 1382 (1995).
24. S. Suzer, *Pure and Applied Chemistry* **69**, 163 (1997).
25. L. Kövér *et al.*, *Surface and Interface Analysis* **23**, 461 (1995).

CJK gratefully acknowledges funding from the National Science Foundation Major Research Instrumentation program (GR# MRI/DMR-1040229). QH and AYB were supported by the U.S. Department of Energy, Office of Science, Basic Energy Sciences, Materials Sciences and Engineering Division and through a user project supported by ORNL's Center for Nanophase Materials Sciences, sponsored by the Scientific User Facilities Division, Office of Science, Basic Energy Sciences, US Department of Energy. GJH gratefully acknowledges funding from the European Research Council (ERC-2011-ADG - Grant Agreement N° 291319 – Acronym "AFTERTHEGOLDRUSH").

Table 1. Direct H_2O_2 synthesis kinetics. Catalytic testing results of the optimized 3wt% Pd – 2wt% Sn / TiO_2 and 2.5wt% Pd - 2.5wt% Au / TiO_2 catalysts after being subjected to various heat treatment regimens.

Entry	Catalyst	H_2O_2 Productivity[a] (+ 2nd use value in brackets) mol kg_{cat}^{-1} h^{-1}	H_2O_2 Degradation[b] mol kg_{cat}^{-1} h^{-1}	H_2 Conversion %	H_2O_2 Selectivity %
	3% Pd - 2% Sn / TiO_2				
1	500 °C / 3 h / air	68 (14)	65	n.d.	n.d.
2	+ Reduced 200 °C / 2 h	60 (60)	300	20	46
3	+ 400 °C / 4 h / air	61 (60)	0	9	96
	2.5% Pd - 2.5% Au / TiO_2				
4	400 °C / 3 h / air	64 (64)	235	22	66
5	+ Reduced 200 °C / 2 h	135	396	n.d.	n.d.
6	+ 400 °C / 4 h / air	82	277	n.d.	n.d.
	1% Pd - 4% Sn / SiO_2				
7	400 °C / 3 h / air	66 (22)	62	n.d.	n.d.
8	+ Reduced 200 °C / 2 h	76 (76)	340	13	70
9	+ 400 °C / 3 h / air	50 (50)	0	8	95

a) Rate of H_2O_2 production determined after reaction using reaction conditions: 5% H_2/CO_2 (2.9 MPa) and 25% O_2/CO_2 (1.1 MPa), 8.5 g solvent (2.9 g HPLC water, 5.6 g MeOH) 0.01g catalyst, 2 ^oC , 1200 rpm, 30 mins.

b) Rate of H_2O_2 degradation calculated from the loss of H_2O_2 using standard reaction conditions: 5%H_2/CO_2 (2.9 MPa), 8.5 g solvent (5.6 g MeOH, 2.22 g H_2O and 0.68 g 50% H_2O_2), 0.01 g catalyst, 2 ^oC, 1200 rpm, 30 mins.

n.d. = not determined

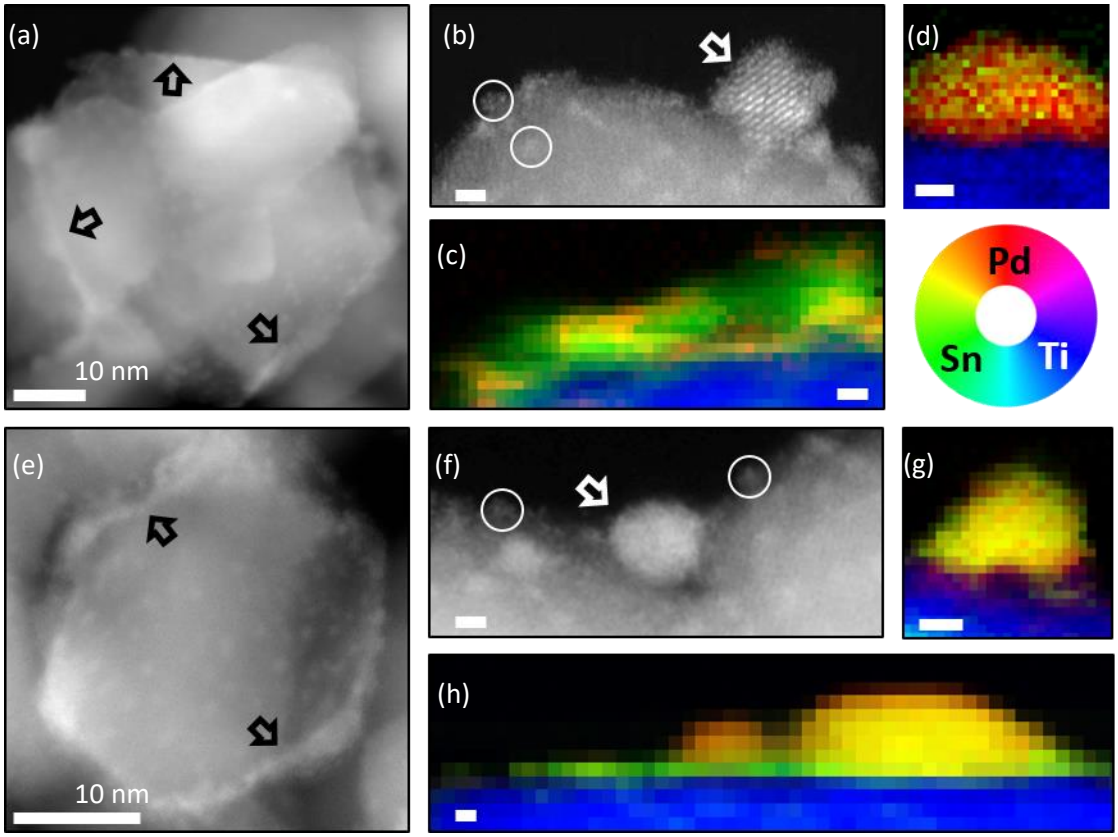

Figure 1. Microstructural analysis of 3wt% Pd – 2wt% Sn / TiO_2 - Representative STEM-HAADF grayscale images and STEM-EELS (RGB) maps of 3wt% Pd – 2wt% Sn / TiO_2 catalysts at (a-d) the oxidized and (e-h) the oxidized-reduced-oxidized stages. From the STEM-HAADF images, three distinct supported species are found in both these catalysts: namely (i) relatively large (*i.e.* 3-10 nm) nanoparticles (white arrows), (ii) smaller clusters on the nm or sub-nm scale (white circles), and (iii) continuous film covering the TiO_2 support surface. The qualitative elemental distribution of Pd, Sn and Ti are represented by red, green and blue respectively in the STEM-EELS maps. (d) and (h) show that the continuous film mainly contains Sn, which either supports or embeds the smaller Pd-rich species. (c) and (g) demonstrate that the larger particles are Pd-Sn alloys. Scale bars in the images and maps represent 1 nm unless noted otherwise.

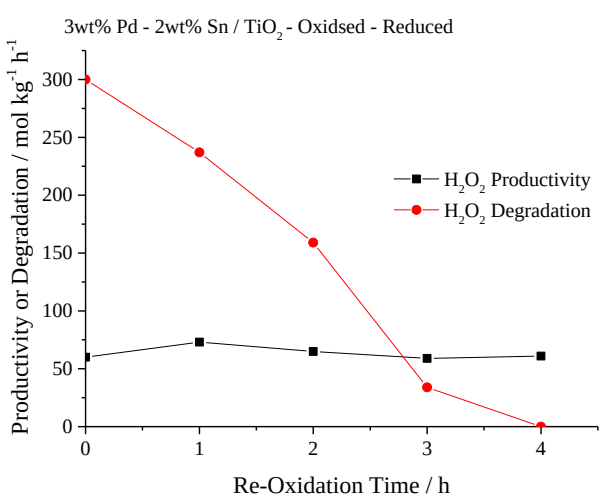

(a) Effect of re-oxidation time under static air at 400 °C on H_2O_2 synthesis and H_2O_2 degradation activity for oxidised-reduced 3wt% Pd - 2wt% Sn / TiO_2 catalyst**.**

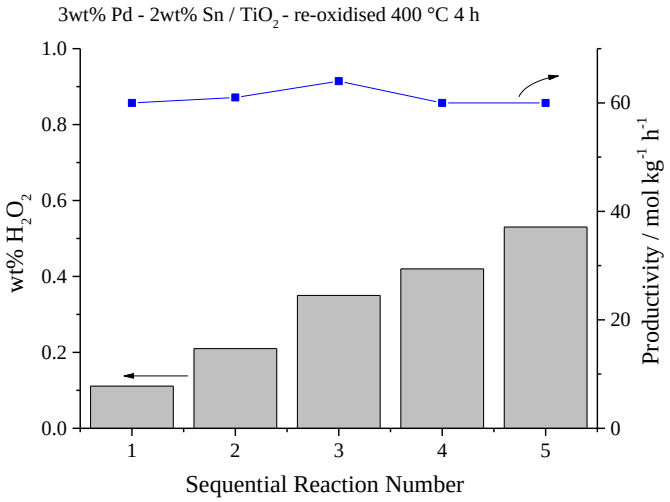

(b) Sequential H_2O_2 synthesis reactions over the 3wt% Pd - 2wt% Sn / TiO_2 material after oxidation-reduction-oxidation treatment.

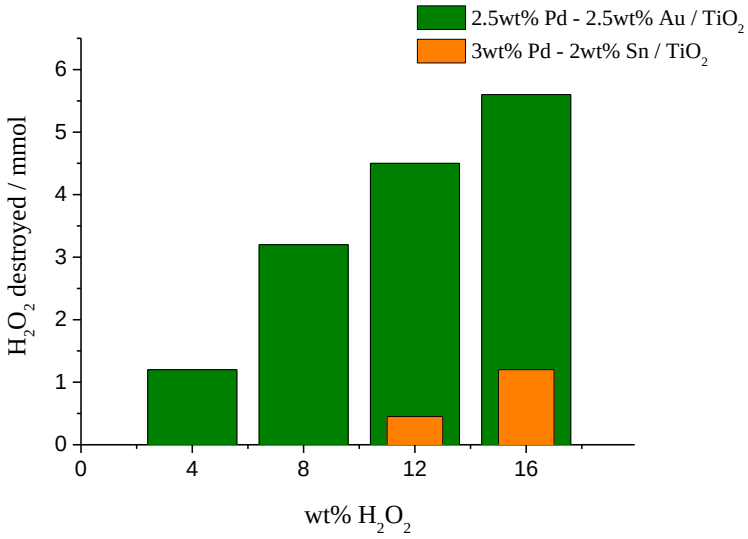

(c) Degradation activity of optimized oxidised-reduced-oxidised 3wt% Pd - 2 wt% Sn / TiO_2 catalyst compared to 2.5wt% Au-2.5wt% Pd / TiO_2 *(8)*

Figure 2. –H_2O_2 direct synthesis and degradation testing of 3wt% Pd - 2wt% Sn / TiO_2

Experimental conditions reported in Table 1 for figure 2 (a-c)

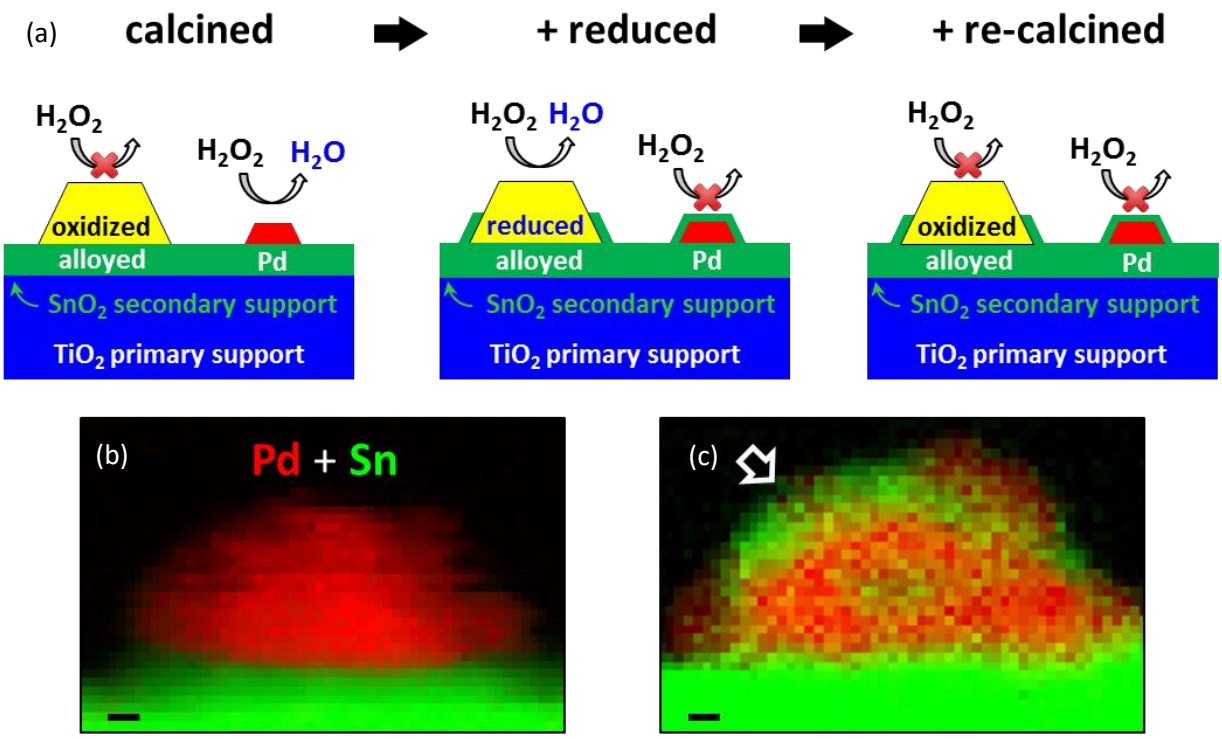

Figure 3. Evolution of catalyst through oxidation-reduction-oxidation cycle (a) Proposed mechanism for switching-off H_2O_2 hydrogenation by small Pd-rich NPs through a strong metal support interaction (SMSI). The secondary metal must form both an alloy with Pd and oxidize to form a secondary support (*i.e.* SnO_x) that can encapsulate the relatively small, poorly alloyed, Pd-rich NPs after an oxidation-reduction-oxidation cycle. This step prevents these NPs from decomposing/hydrogenating the H_2O_2 product. STEM-EELS mapping of a 5wt% Pd / SnO_2 model catalyst at the **(b)** oxidized and **(c)** oxidized-reduced-oxidized stages, showing partial encapsulation of the Pd NP (red) by SnO_x (green) after the oxidation-reduction-oxidation heat treatment cycle. The Sn intensities in the SnO_2 support area were deliberately saturated to show up any relatively weak signals in the particle region. The scale bars represent 1 nm.